Journal of
Ceramic Science
and Technology

J. Ceram. Sci. Tech., 02 [01] 1-8 (2011)
DOI: 10.4416/JCST2010-00018
available online at: http://www.ceramic-science.com

Development of a Technology for the Obtainment of Fine Grain Size, Transparent $MgAl_2O_4$ Spinel Parts

A. Goldstein*, A. Goldenberg, M. Vulfson

Israel Ceramic and Silicate Institute, Technion City, Haifa 32000, Israel
received May 25, 2010; received in revised form July 12, 2010; accepted September 23, 2010

Abstract

The objective of the work was the establishment of a procedure allowing the obtainment of high-optical-transparency $MgAl_2O_4$ polycrystalline parts that exhibit a fine microstructure (average grains size lower than 5 µm). The technology had to be relevant for industrial-scale production. A nano powder, commercially available in large quantities, at a reasonable price, was used as raw material. It was determined that by applying a suitable combination of powder processing and green-bodies-forming procedure, a configuration favorable for advanced densification can be derived from the selected powder. It was also found that the pore-closing ability of HIPing was best exploited when the specimens subjected to this treatment (predensified by pressureless sintering, in air) exhibited an optimal tradeoff between densification level and microstructural configuration. Specimens combining an average grain size of 2.5 µm with an in-line transmission of 77 % (λ = 750 nm; thickness ~2 mm) were obtained; such parts possess a Vickers hardness of 13.8 GPa and a transverse rupture strength of ~200 MPa. Because the technology developed generates transparent spinel exhibiting properties acceptable for some of the existent applications, at reasonable cost, it may be of interest to industry.

Keywords: Spinel, transparent, ceramic, sintering, armor

I. Introduction

Transparent (energy gap ≅ 7.8 eV) $MgAl_2O_4$ spinel finds use in a number of applications, like protective domes for infrared sensors, armor, barcode reader heads, pressure vessel windows, laser-based spark plugs, or microlithography lenses [1-6]. It was first obtained as single crystal, and then – by powder sintering – as polycrystalline (TPS) parts [2-26].

The essential parameter for performance estimation is the optical in-line transmission (ILT), which is desired to be as close as possible to the theoretical limit of ~87 % (~0.3 - 5 µm range) [5,15]. The minimal acceptable level varies from application to application (being, though, rarely lower than 70 %), and so does the relevant wavelengths range (VIS, MIR or near-UV).

Besides transparency, of considerable importance is a fine microstructure [5,27,28]. Lowering the grain size improves the mechanical properties and thermal shock resistance [4-6,29]. In the particular case of armor, it also accelerates projectile erosion [28].

A number of technologies have been developed, over the years, for the fabrication of TPS-based products [2-34]. In most of these technologies a powder compact is sintered to full density, either by pressureless sintering (AS) followed by hot isostatic pressing (HIP), or hot pressing (HP) followed by HIPing. Interesting results have also been obtained with fusion casting [30]. Some of these procedures are able to deliver spinel parts of excellent transparency, large size and desired shape. The microstructure of these components is, however, in most cases, coarse, being based on grains of a size >> 10 µm.

Attempts have also been made, mostly in recent years, to develop TPS that combines high transparency with a fine microstructure (average grain size $\overline{GS}$ in the 1.5 – 10 µm range) [3,14,24,25,27,31-34]. The feasibility of obtaining even submicron $\overline{GS}$ coupled with an ILT ≥ 80 %, was demonstrated by Krell et al and then Goldstein et al [20,21]. None of the resulting procedures, for fine-grained TPS obtainment, are used for industrial production, owing to various drawbacks, like the need for an excessively complex hot pressing stage, achievement of insufficient transparency, low size of obtainable parts, the need for additives, expensive raw materials, only partial disclosure of technology, etc.

The goal of this work was to develop a technology allowing the obtainment of fine microstructure, highly transparent (T ≥ 75 %) spinel parts, which can be used (being low-cost enough) for industrial scale fabrication. For this, first, a powder commercially available, at a reasonable price and in large quantities, was selected (from a quite meager set of options). A procedure, including powder processing, forming and sintering (an AS+HIP approach, which is significantly less costly than a HP+HIP one), allowing the conversion of this powder into TPS, was then established; the densified parts have been characterized regarding microstructure, optical and mechanical properties. Obtainment of TPS from this type of powder was ex-

* Corresponding author: goldaad@actcom.net.il

amined previously, especially in the US and Taiwan, but in most cases technologies generating parts exhibiting a large grain size were established [10,13,15,16,18]. Submicron-grained TPS exhibiting excellent mechanical properties was also obtained lately in Germany [35], but the specifics of the procedure used (especially sintering aids) were not disclosed.

II. Experimental

The raw material selected is prepared, from pure Al and Mg sulphates, by Baikowski (La Balme de Silligny, France) using wet chemistry followed by calcination and jet milling. Its main impurities are (in ppm) S 200, Ca 80, Fe 30, Na 50, K 35. A = 29 m^2/g. It has a composition corresponding to a 1 : 1 molar ratio of MgO and Al_2O_3. The powder includes only the cubic $MgAl_2O_4$ spinel (JCPDS card 21-1152).

The powder, suspended in ethylene glycol (diluted suspension), was deagglomerated by ultrasonication, in the presence of a deflocculant suitable for organic solvents, and pelletized by the aid of a 71-mesh sieve. The pellets were spheroidized by tumbling. Green parts have been formed by cold isostatic pressing (CIP), following a schedule which includes a number of dwells both during the increase and decrease of the pressure. During the raising and decreasing of pressure, 10 min dwells were kept at 80, 140 and 200 MPa (maximal pressure). Most of the specimens were disc-shaped (diameter ϕ_i = 25 to 60 mm; thickness t_i = 3 to 6 mm; i = initial), but a number of plates were also formed (l_i = 40 to 60 mm). Isothermal sintering in air (AS) was effectuated by maintaining 3-h dwells at different temperatures ($t°_s$ = sintering temperature) in the 1250 – 1650 °C range. The final densification stage was performed by the aid of an in-house made HIP, under Ar, at ~ 200 MPa, at various temperatures in the 1400 to 1600 °C range, keeping, in all cases, a 3-h dwell at the peak temperature. Gray coloration, present after HIPing in most of the specimens, was eliminated by annealing in air (1250 – 1280 °C range; 2-h dwell).

The bulk density of the powder compacts was labeled BD_g, that reached after air sintering (3-h dwell) - BD_A; the bulk density after HIPing was labeled BD_H. They were determined by means of the Archimedes technique (for BD_g the powder compact was strengthened by heating to 850 °C/2 h).

The powder particles (agglomerates) size distribution (dispersion in ethylene glycol) was measured with the aid of a laser-diffraction-based sizer (model Mastersizer 2000, from Malvern Instruments, Worcestershire, UK). The pore size distribution (green body strengthened by heating at 850 °C/2 h) was measured by mercury intrusion (model Macropore 120 porosimeter from Carlo Erba, Torino, Italy).

The phase composition of the raw materials and densified specimens was determined from diffractograms obtained with the aid of an X-ray diffractometer (XRD; model APD from ItalStructures, Riva del Garda, Italy). This machine uses the CuKα-1 radiation (λ = 1.5406 Å); peaks present in the diffractograms were identified with the aid of JCPDS cards.

Powder morphology was examined with TEM (model TECNAI G^2, T-20, from FEI, Eindhoven, NL) while the microstructure of the sintered parts was illustrated by SEM (model Quanta 200, FEI). The average grain size ($\overline{GS}$) was measured with the aid of the mean lineal intercept method, using the approximation GS=1.5$\overline{L}$, where $\overline{L}$ is the mean intercept (ASTM E-112-88). At least 200 grains, located on three different specimens, were measured.

The hardness, under a load of 5 kg (HV5), was measured with the aid of a Vickers indenter (model DVK-1 of Matsuzawa, Tokyo, Japan).

Young's modulus (E) was derived from sound speed measurements (pulse echo technique, 5 MHz probe).

The transverse rupture strength (TRS) was measured using a three-point-bending configuration (L = 27 mm, H = 5.1 mm, W = 4.3 mm; 34 kg/min loading rate) on a set of 12 polished test bars; the Weibull modulus "m" was also determined. Owing to the small number (12) of strength measurements available, the confidence level one may associate with the result regarding "m" is moderate (for high confidence more than 100 measurements would be needed); the value obtained is only orientative.

The optical transmission spectra were recorded by a double-beam spectrophotometer (model Lambda 950 from Perkin Elmer, Shelton, CT, USA) on polished specimens (t = 1.7 mm). In order to eliminate the scattered component of the light beam, a 4 x 4-mm slit was located between the specimen and detector, as recommended by Dercioglu et al. [17], so that the values shown may be considered as in line transmission ones.

III. Results and Discussion

(1) Optimization of green body configuration

Comparison of the results of some of our previous works [3,21] and the literature [20] suggest that a significant increase in sinterability can be obtained by improving the configuration of spinel powder compacts at the nano- and micro-scale. Those results and theoretical examination of the green body structure/sinterability correlation [7, 36,37] indicate that in a good configuration the average pore size should be as low as possible and the size distribution should be narrow. The latter requirement stems from the need for keeping the interaggregate pores size in the same range with the intraaggregate voids (the interaggregate pores, being the largest, control the maximal attainable densification level). The pore coordination number (by particles) has to be as low as possible (to allow, thermodynamically, pore shrinkage [7]) and the curvature of the particles high. The agglomerates' internal porosity, size, shape, tribological behavior during forming (a factor difficult to measure and usually overlooked) and arrangement compactness have to be such as to allow the formation of the desired configuration and to minimize the deterioration – of the initial green body pores size distribution – inevitably produced, by differential densification, in the first stage of sintering [36]. The residual mechanical stress, existent after forming, has to be low enough so as not to cause cracking and/or change in the voids' size and shape during relaxation (e.g. spring effect of particles elastically deformed by excessive pressing force). A low amount of

porosity, i.e. a high BD_g, is also helpful, but only if it is not obtained by negatively affecting one or more of the porosity characteristics listed above. Last but not least, the local nano- and micro-scale configuration has to be uniformly repeated throughout the macroscopic volume of the specimen.

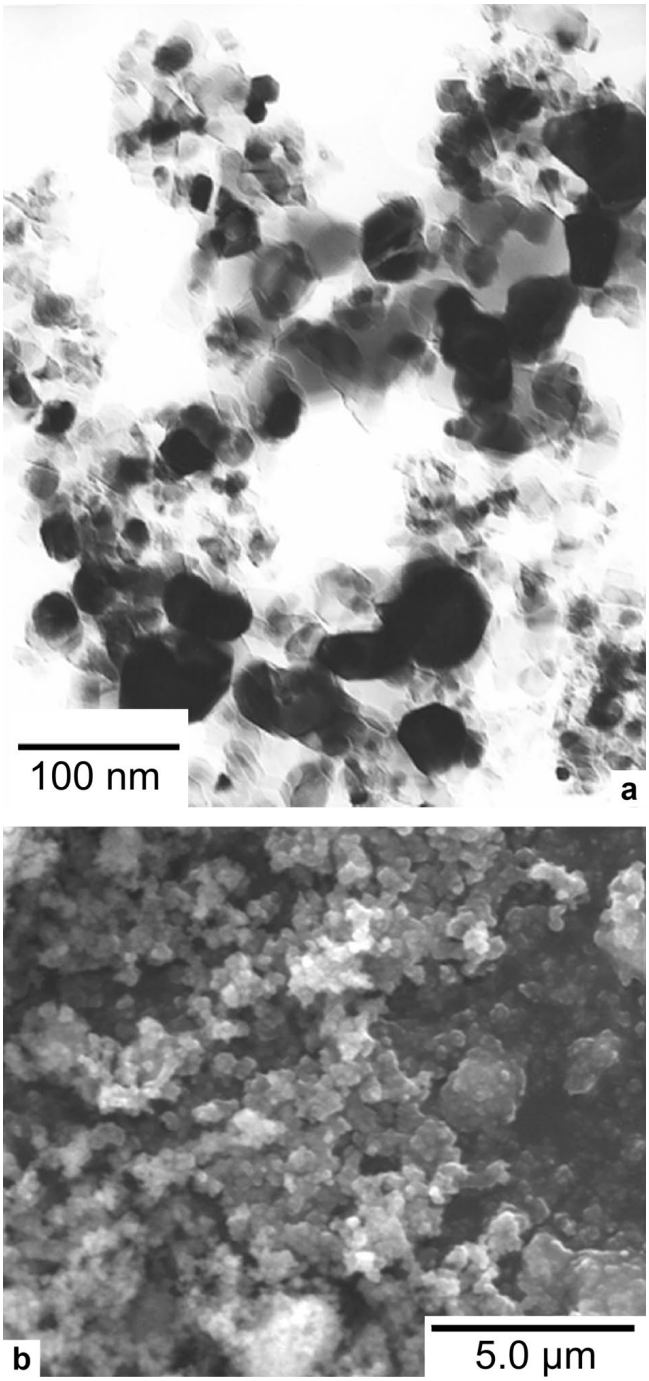

Fig. 1: Ultimate particles and agglomerates of SCR-30 grade $MgAl_2O_4$ powder.
(a) Ultimate particles size, morphology and clustering pattern. TEM.
(b) Size and morphology of multilevel aggregates (particles). SEM.

The morphology of the ultimate particles of the powder used here and its initial clustering pattern are shown in Fig. 1a. The faceted (unfortunately not spheroidal) crystallites (average size of 45 nm) aggregate to form multilevel agglomerates of variable size and shape. As the figure shows, the primary clusters include crystallites strongly linked over grain boundaries, formed by diffusion (during powder synthesis). Those clusters further coalesce into higher level agglomerates, mostly owing to the action of van der Waals forces, of up to a few microns in size.

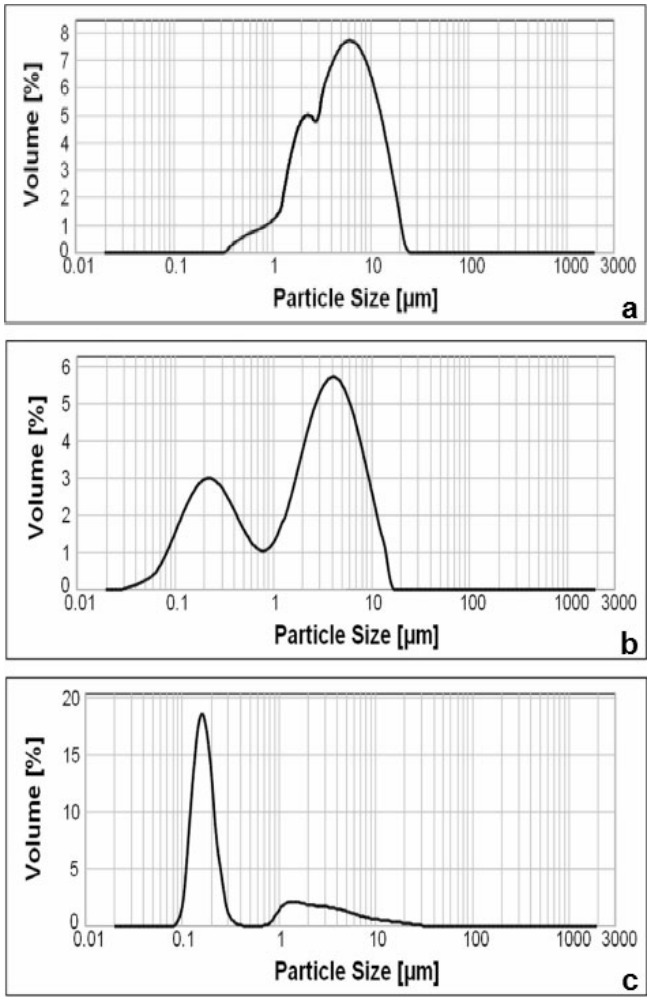

Fig. 2: Spinel powder particles size distribution after different types of processing.
(a) Deagglomeration by ultrasonication in water.
(b) Deagglomeration by ultrasonication in isopropyl alcohol.
(c) Deagglomeration by ultrasonication in ethylene glycol (includes 1.8 % deflocculant operating by steric stabilization mechanism).

Preliminary experiments showed that deagglomeration treatments of the as received powder increase the BD_g and reduce somewhat the pore size distribution width of the green body. Therefore, various agglomerate-breaking techniques, like ball and jet milling, together with ultrasonication, were examined. The latter procedure gave the best results (including an absence of impurification). The performance of the procedure is markedly affected by parameters like: ultrasound source power, suspension volume and solid loading, nature of the suspending liquid and nature of deflocculant. In Fig. 2 the particle size distribution obtained after deagglomeration under various conditions is illustrated. The data in the Figure indicate that when ethylene glycol was used as suspending medium and a suitable dispersant was added, a massive agglomerate size reduction was obtained. Fig. 3 shows the pore size distribution of the green body obtained by pressing the pow-

der with the particle size distribution detailed in Fig. 2c; its BD_g (1.83 g/cm^3) is also indicated (caption). As it may be seen, the pore size (including the interagglomerate ones) is in the same range as that of the basic particles, a situation which permits realization of low pore coordination numbers; the average pore size is quite low, at a value of ~ 40 nm, and the distribution width narrow.

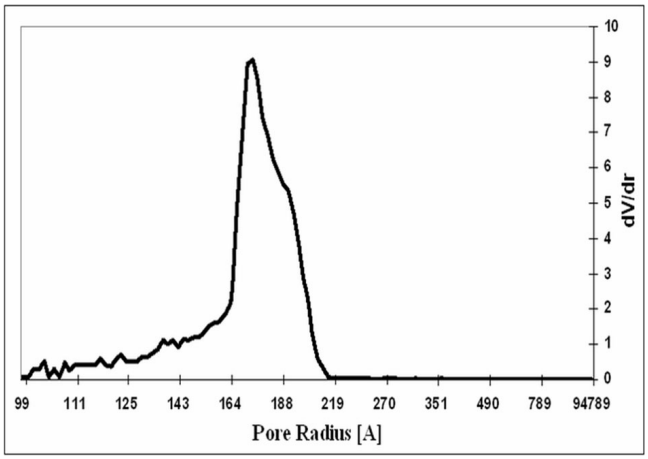

Fig. 3: Pores size distribution of green body formed by pressing of powder having a particles size distribution like that illustrated in Fig. 2c. BD_g = 1.83 g/cm^3 (~ 51 % TD); Mercury intrusion.

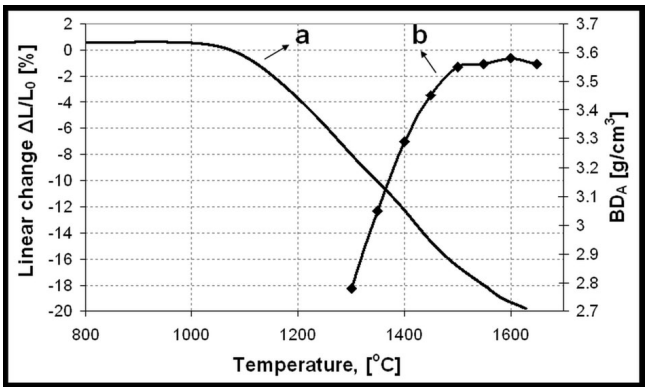

Fig. 4: Sintering shrinkage curve (5 °C/min) and $BD_A = f(t°_s)$ for 3 h dwell isothermal firing. (TD=3.578 g/cm^3).
(a) DL/L·100 = f (temp.)
(b) $BD_A = f(t°_s)$

(2) Pressureless sintering stage

In Fig. 4 the sintering shrinkage is shown together with the evolution, as a function of peak temperature, of the BD_A of specimens subjected to isothermal sintering using 3-h dwells. The dilatometric curve (Fig. 4a) shows that densification starts as low as 1100 °C, but attains its maximal level at the relatively high temperature of 1620 °C, after shrinkage of ~ 20 %. As Fig. 4b shows, BD_A values (BD_A = 3.575 g/cm^3; 99.9 % TD) very close to the theoretical density (TD = 3.578 g/cm^3) can be obtained by isothermal pressureless sintering at 1600 °C, with 3-h dwell times, but optically this brings about only a slight translucency, i.e. a level of transmission far below that required by the applications. The low transmission, even at such high BD_A values, is a consequence of the light scattering produced by the residual porosity. Residual porosity, after AS, exists owing to the fact that as it is approaching completion, the ionic-diffusion-based densification process slows down strongly as a result of grain growth and consequent pore size increase (coalescence), as indicated by the experimental work and also equations (1) and (2), which show the strong dependence of the densification rate on GS [37-40].

$$\frac{d\rho}{d\tau} = \frac{441 D_L \gamma_S V_m}{RT\,GS^3}(1-\rho)^{\frac{1}{3}} \quad (1)$$

and/or

$$\frac{d\rho}{d\tau} = \frac{733 \delta_B D_B \gamma_S V_m}{RT\,GS^4} \quad (2)$$

where:
ρ is the density;
τ is the time;
$D_{B.\,L}$ are the lattice and grain boundary diffusion coefficients;
γ_S is the surface energy;
V_m is the molar volume;
R is the gases constant;
T is the absolute temperature;
δ_B is the GB (grain boundary) width;

The relative contribution to densification of the two types of diffusion varies with temperature and grain size.

The grains growth also causes the formation of a fraction of occluded porosity (its closure is more difficult than that of GB attached voids) over a critical density, ρ_C, [41] which in the case of pore drag control (prevalent in the case of pure powders) is:

$$\rho_C = 1 - \left[\frac{\varepsilon}{3.3}\left(1 - \frac{\overline{GS}}{GS_M}\right)\right]^3 \quad (3)$$

where:
ε is a constant which allows for different limiting cases in the GS distribution;
$\overline{GS}$ is the average and GS_M the maximal grain size.
The value of ρ_C is seen to be dependent also on the microstructural pattern, like $\frac{d\rho}{d\tau}$.

In Fig. 5 the microstructure of the specimens which attained, after AS, respectively, 96.5 % TD and 99.9 % TD, is shown. The $\overline{GS}$ (see Table 1) has risen from 1.8 to 3.8 µm. More importantly, the largest grains grew from 4.5 to 12 µm. The size increase, especially of the largest grains, while not massive, is significant enough to contribute, for reasons mentioned above, to densification slow-down.

Owing to the above, the end-point of pressureless densification is attained quite close to TD, but still **before** the residual porosity is lowered under the maximal limit of ~ 300 ppm required (together with a pore size ϕ which satisfies either $\lambda/\phi > 10$ or $\phi >> \lambda$) for reducing scattering enough to make high transparency achievement possible [42]. As a result, the specimens are only translucent at the end of the AS stage. In order to attain the desired levels of optical transmission, further sintering, under conditions ensuring a stronger drive toward pore closure than AS is able to offer, is needed. Such conditions are provided by HIPing.

Table 1 Optical transmission of disks (t_f = 1.7mm), obtained by AS+HIP 1520 °C/3 h (annealing in air 1280 °C/2 h), as a function of the AS temperature (1420-1650 °C range) and characteristics of as-ASed specimens.

After air Sintering					After HIP at 1520 °C
Temperature	$\overline{BD}_A$	Total residual porosity (TP)* (all of it is closed)	$\overline{GS}$	GS_M**	In-line transmission λ = 750 nm
°C	g/cm³	%	µm	µm	%
1420	3.340±0.007	6.70	1.20±0.35	3.00	<40
1450	3.450±0.005	3.60	1.85±0.82	4.50	75
1470	3.470±0.003	2.75	1.80±0.74	4.00	77
1500	3.540±0.006	1.00	2.25±0.38	4.50	77
1550	3.560±0.007	0.50	2.50±0.26	5.00	74
1600	3.575±0.008	0.10	3.80±0.27	12.00	72
1650	3.565±0.006	0.40	4.35±0.32	12.00	68

* TP calculated from BD_A values (TD=3.578 g/cm³)
** GS_M = maximal grain size

The driving force for pore closure in the final stage of AS is, for oxides, in the region of 2 to 20 MPa, depending on their size and γ_S [43]. If an external pressure (P) is applied, the densification rate becomes [41].

$$\frac{d\rho}{d\tau} = 31.5 \frac{V_M}{kT\overline{GS}^2} (1 - \rho) \left[D_L + \frac{\pi \delta_B D_B}{\overline{GS}} \right] P \qquad (4)$$

where:
k is the Boltzman constant;
P is external pressure.

The positive effect of P on pore closure may be quite significant, bearing in mind that in the HIP machines P may reach 200 – 300 MPa. The effect is stronger on pores connected to GBs, but it is also felt by occluded pores because the chemical potential of the ionic specimens located at GBs close to the pore is increased and the pore gas pressure is opposed (possibly, the mobility of dislocations close to the pore is raised).

(3) Achievement of transparency by HIPing

For HIPing, without encapsulation, the specimens have to exhibit very low open porosity. In this work only specimens having OP ≈ O (i.e. sintered at t° ≥ 1420 °C) were subjected to HIPing.

After HIPing at temperatures ≤ 1450 °C, only opaque or translucent specimens were obtained. Interestingly, specimens produced by AS in the 1450 to 1500 °C range were, after HIPing, somewhat more translucent than those sintered at higher temperatures (1550 up to 1650 °C).

The lowest HIPing temperature that produced specimens with an ILT ≥ 60 % was 1520 °C. In Table 1 the BD_A, $\overline{GS}$ and total residual porosity (TP), after the pressureless sintering stage, are listed, together with ILT values after HIPing at 1520 °C. As it may be seen, ILT increases when the AS temperature of the specimens subjected to HIPing is raised from 1420 to 1470 °C. A further increase in sintering temperature, though, does not improve the transmission (even some decrease is observed above 1500 °C), despite the fact that the BD_A increased continuously in

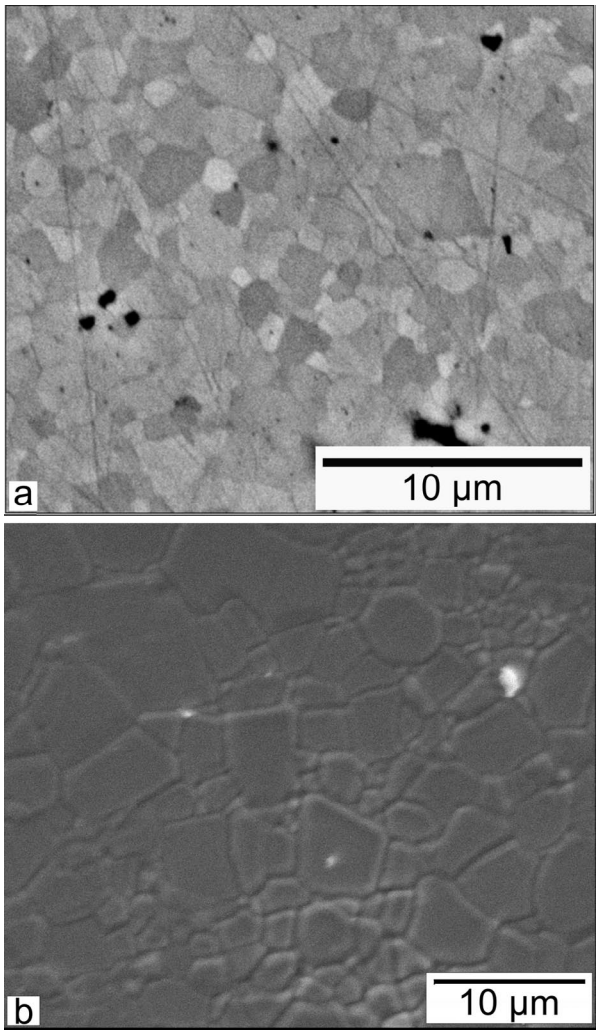

Fig. 5: Microstructure of spinel parts after AS (3 h) at temperatures which generate parts with a BD_A of respectively 96.5 and 99.9 %TD.
(a) BD_A=96.5 %TD ($t°_s$ = 1450 °C) = 1.8 mm (chemical etching with H_3PO_4 solutions; BSE).
(b) BD_A=99.9 %TD ($t°_s$= 1600 °C) = 3.8 mm (thermal etching at 1450 °C/40 min; SE).

the 1420 to 1600 °C domain. A specimen ASed at 1470 °C has, after HIPing at 1520 °C, a $\overline{GS}$ = 2.5 µm. Increase of the HIPing temperature – for the case of parts ASed in the 1470 – 1500 °C range – to 1580 °C, while improving transparency (see Fig. 6 and Fig. 7), so that ILT rises to 83 %, also causes slight grain growth; the $\overline{GS}$ (specimen ASed at 1470 °C) rises from 2.5 to 3.5 µm as a result of such a HIPing temperature increase. The results of Table 1 suggest that the amount of porosity, after AS (BD_A, TP), is not the only factor affecting behavior during HIPing. Increase of

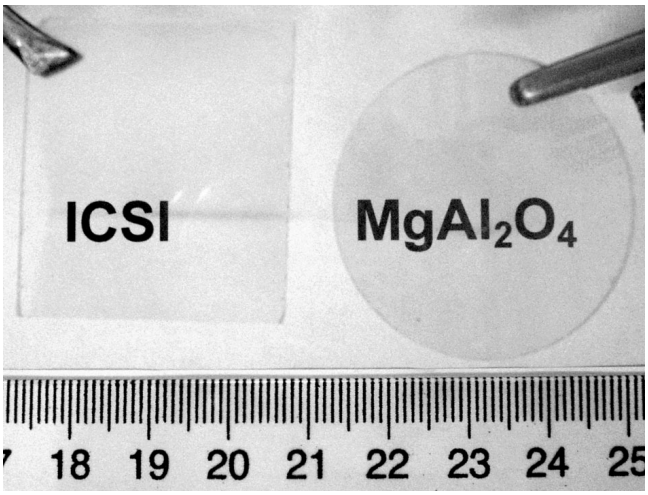

Fig. 6: Illustration of spinel parts that underwent the AS+HIP densification process (t = 2 mm).
Square: AS 1470 °C+HIPing at 1580 °C
Disk: AS 1470 °C+HIPing at 1520 °C
Specimens held 2 cm above background

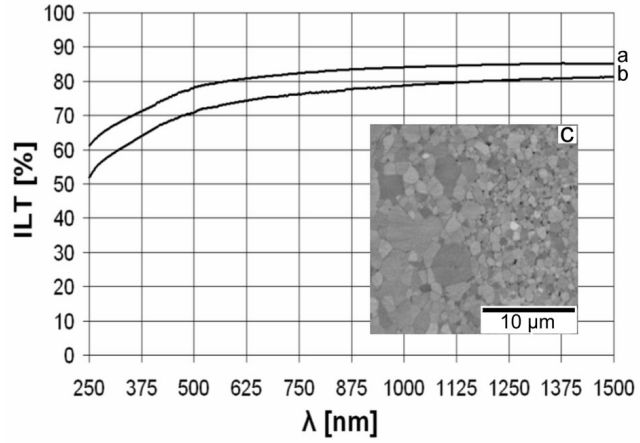

Fig. 7: ILT as a function of λ (250 - 1500 nm domain) of disks (t = 1.7 mm; AS = 1470 °C) HIPed at two different temperatures (the microstructure after HIPing at 1520 °C is also shown).
(a) HIP at 1580 °C
(b) HIPed at 1520 °C
(c) Microstructure of specimen made by AS 1470 °C/3 h+HIPing 1520 °C.
SEM; $\overline{GS}$=2.5 µm (chemical etching with H_3PO_4 solutions; BSE).

the AS temperature from 1420 to 1600 °C, while continuously reducing TP, also caused a noticeable, albeit not massive, microstructure coarsening. The increase of the fraction of occluded porosity, its size and distance from GBs, as the BD_A approaches the TD and coarsening progresses, accompanied also by a size increase of some of the GB connected pores (those resulting by pore coalescence), makes pores closure more difficult, despite the reduction of their total amount. The most efficient pore closure during HIPing is obtained in the case of specimens exhibiting an optimal tradeoff between TP and the pore system characteristics (size and location). Here this is achieved for specimens ASed in the 1470 – 1500 °C range. A similar behavior was observed also by Tsukuma and Kwon [24,44]. The observation that specimens sintered in the 1470 – 1500 °C range exhibit, after HIPing, an optical transmission not worse (but in fact slightly higher) than those fired at 1600 °C, helps one to reduce the GS of the TPS.

In Fig. 7 the transmission curve of disks (t = 1.7 mm) sintered at 1470 °C and HIPed at, respectively, 1520 and 1580 °C, are shown. The higher HIPing temperature further reduces porosity (stronger diffusion), so that the ILT is increased by ~ 6 %.

Most of the small-size disks (ϕ ~ 20 mm) were free of microdefects, but in larger specimens (L > 30 mm) some opaque spots (10 to 100 µm in size) were randomly distributed (Fig. 8) in the otherwise highly transparent matrix. The size and number of such defects tend to increase with the size and thickness of the specimens. While not always affecting transmission measurements, such defects are deleterious.

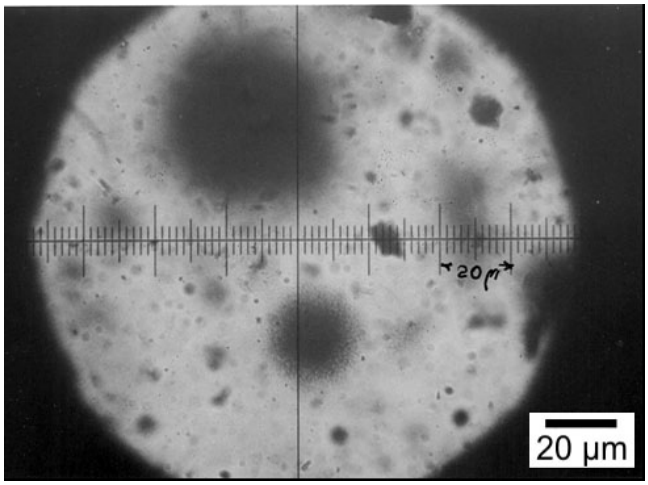

Fig. 8: Size, shape and clustering pattern of micro opaque spots within transparent spinel matrix. Optical microscopy.

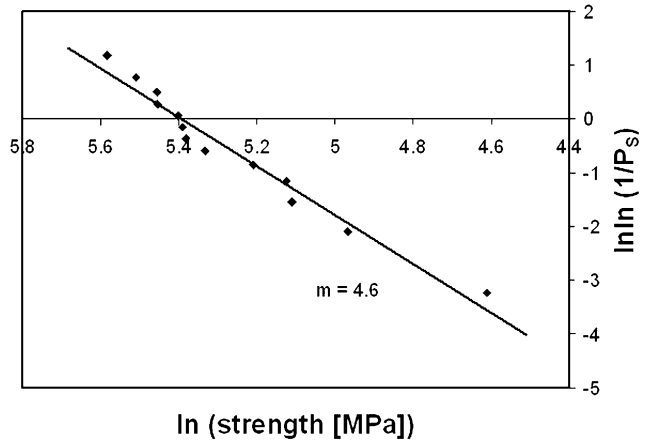

Fig. 9: Survival probability (P_S) as a function of rupture strength (ln-ln format for Weibull modulus "m" calculation).

(4) Mechanical properties

In Table 2 the average values measured for GS, ILT, HV5, TRS and E are given. For comparison, the values measured on specimens derived from a powder prepared by flame spray pyrolysis (FSP) are also given; those specimens have a submicron grain size, obtained by low-temperature HIPing (at 1320 °C) parts sintered in air at 1280 °C [21]. The strength is reasonable, similar to values obtained by others [2] but the low value of "m" (Fig. 9) indicates that further improvement of reliability is needed. As the table shows, the coarser microstructure of the specimens developed in this work reduces the hardness, but not drastically (~ 5 %). The reduction is more marked if the HV5 values obtained here are compared with those reported in [35], where a powder from the same supplier as the one relevant here was used to obtain submicron-grained TPS. There, for $\overline{GS}$ = 0.42 µm, the Vickers hardness is similar to that found in [21] (HV10 = 14.6 GPa), but the value is obtained under a 10 kg load. While the information about processing given in [35] is not detailed enough to allow replication (or estimate costs), the results presented there indicate that higher performance than that obtained here is attainable with optimized technology. The GS could be reduced there to under 1 µm (the optimal microstructure for armor), while the ILT is almost theoretical.

Table 2: Optical transmission and mechanical properties of HIPed TPS.

Spinel powder type	$\overline{GS}$ µm	In-line transmission (t=1.7mm) %	$\overline{HV5}$ GPa	$\overline{TRS}$ MPa	$\overline{E}$ GPa
SCR-30	2.50±0.94	77	13.8±0.3	200±58 (m=4.6)	290±10
FSP (for fabrication procedure – see [21])	0.45±0.36	80	14.5±0.2		290±10

IV. Conclusions

If the selected spinel powder is subjected to suitable processing and forming procedures, green bodies, exhibiting nano-size pores (with a quite narrow size distribution), i.e. a configuration favorable for sintering, are obtained. Owing to the marked influence that green body configuration has on sintering, the powder compacts obtained could be densified, by pressureless sintering in air, to a level of 99.9 % of the theoretical density. After HIPing, parts exhibiting a transmission of up to 83 % (λ = 750 nm), combined with a $\overline{GS}$ not larger than 3.5 µm (or an ILT of 77 % combined with $\overline{GS}$ = 2.5 µm), could be produced. The HIPing is most efficient when sintered specimens exhibiting an optimal tradeoff between the amount of residual porosity and the pore size and location (connected to GBs or occluded), are subjected to this treatment. This fact contributes to the reduction of the TPS grains' size. Such a tradeoff is obtained for BD_A values in the 97 - 98.5 %TD. The technology defined here can be relevant for commercial production, because it generates TPS parts with quite high performance (lower, but not far away from that attained in [35]) using a moderate cost raw material and low-cost (compared to the HP+HIP approach) processing. The main objective of further work is the total elimination of the residual micro opaque spots in large specimens.

References

1 Woosley, J.D., Wood, S., Jander, E., Weeks, R.A.: Photoelectric effects in $MgAl_2O_4$ spinel, *Phys. Rev.*, **22**, 1065, (1980).

2 Harris, D.C.: History of development of polycrystalline optical spinel in the US, Proc. SPIE, **5786**, 1-22, (2005).

3 Goldstein, A., Goldenberg, A., Yeshurun, Y., Hefetz, M.: Transparent $MgAl_2O_4$ spinel from a powder prepared by flame spray pyrolysis, *J. Am. Ceram. Soc.*, **91**(12), 4141-4144, (2008).

4 Reimanis, I., Kleebe, H.J.: A review on the sintering and microstructure development of transparent spinel ($MgAl_2O_4$), *J. Am. Ceram. Soc.*, **92**(7), 1472-1480, (2009).

5 Krell, A., Hutzler, T., Klimke, J.: Transparent ceramics for structural applications: part 2, fields of application, *cfi Ber. DKG*, **84**(6), E50-E56, (2007).

6 Cox, J.A., Greenlow, D., Terry, G., Fiedler, L.: Comparative study of advanced IR transmissive materials, Proc. SPIE, **683**, 49-61, (1986).

7 Kingery, W.D., Francois, B.: Sintering of Crystalline Oxides I, In: Sintering and Related Phenomena. Kuzcsynski,G.C., Hooton, N.A. and Gibbon G.F. eds, Gordon and Breach, New York, (1967), p. 471.

8 Bratton, R.J.: Translucent sintered $MgAl_2O_4$, *J. Am. Ceram. Soc.*, **57**(7), 283-286, (1974).

9 Roy, D.W., Hastert, J.L.: Polycrystalline $MgAl_2O_4$ spinel for high temperature windows, *Ceram. Eng. Sci. Proc.*, **47**(7-8), 502-509, (1983).

10 Hsu, S.E., Wang, C.T., Tsai, D.S., Yang, S.J.: Effect of gas pressure on optical quality of $MgAl_2O_4$ spinel, Mat. Res. Soc. Symp. Proc., **251**, 257-264, (1992).

11 Roy, D.W., Hastert, J.L., Canbrough, L.E., Green, K.E., Trujillo, A.: Transparent Polycrystalline Body with High UV Transmittance, Process for Making, and Applications Thereof. European Patent 0447390B1, (1994).

12 Bergez, P.: Procedé de Fabrication de Pieces en Spinelle d'Aluminate de Magnesium à Hautes Performances Notamment de Pièces Transparents dans le Domaine de Infrarouge et Visible. European Patent 0334760B1, (1993).

13 Roy, D.W.: Hot pressed $MgAl_2O_4$ for UV visible and infrared optical requirements, Proc. SPIE, **297**, 13-18, (1981).

14 Gazza, G.E., Dutta, S.K.: Transparent Ultrafine Grained Ceramics. U.S. Patent 4, 029, 755, (1977).

15 Gilde, G., Patel, P., Patterson, P., Blodget, D., Duncan D., Hahn, D.: Evaluation of hot pressing and hot isostatic pressing parameters on the optical properties of spinel, *J. Am. Ceram. Soc.*, **88**(10), 2747-2751, (2005).

16 Cheng, J., Agrawal, D., Zhang, Y., Browl, B., Roy, R.: Fabricating transparent ceramics by MW sintering, *Am. Ceram. Soc. Bull.*, **79**(9), 71-74, (2000).

17 Dercioglu, A.F., Kagawa, Y.: Effect of grain boundary microcracking on the light transmittance of sintered transparent $MgAl_2O_4$, *J. Eur. Ceram. Soc.*, **23**, 951-959, (2003).

18 Mroz, T.J., Hartnett, T.M., Wahl, J.M., Goldman, L.M., Kirsch, J., Lindberg, W.R.: Recent advances in spinel optical ceramics, Proc. SPIE, **5786**, 64-70, (2005).

19 Goldstein, A., Geifman, L., Bar-Ziv, S.: Susceptor-assisted microwave sintering of $MgAl_2O_4$ powder at 2.45 GHz, *J. Mat. Sci. Lett.*, **17**(12), 977-979, (1998).

20 Krell, A., Hutzler, T., Klimke, J.: Transparent ceramics for structural applications: part 1, physics of light transmission

and technological consequences, *cfi Ber. DKG*, **84**(4), E41-E50, (2007).

21 Goldstein, A., Goldenberg, A., Hefetz, M.: Transparent polycrystalline $MgAl_2O_4$ spinel with submicron grains, by low temperature sintering, *J. Ceram. Soc. Jpn.*, **117**(11), 1281-1283, (2009).

22 Meir, S., Kalabubkhov, S., Froumin, N., Dariel, M.P., Frage, N.: Synthesis and densification of transparent $MgAl_2O_4$ spinel by SPS process, *J. Am. Ceram. Soc.*, **92**(2), 358-364, (2009).

23 Lei, M.Y., Huang, C.X., Sin, J.L.: Effect of HIP on the properties and microstructure of transparent polycrystalline spinel, *Key Eng. Mat.*, **336-338**, 1200-1202, (2007).

24 Tsukuma, K.: Transparent $MgAl_2O_4$ spinel ceramics produced by HIP post-sintering, *J. Cer. Soc. Jpn*., **114**(10), 802-806, (2006).

25 Sweeney, S.M., Brun, M.K., Yosenick, T.J., Kebbede, A., Manohora, M.: High-strength transparent spinel with fine unimodal grain size, Proc. SPIE, **7302**, 73020G, (2009).

26 Villalobos, G.R., Sanghera, J.J., Bayya, S.S., Aggarwal, I.: Magnesium aluminate transparent ceramic having low scattering and absorption loss. WO Patent 2006/104540, (2006).

27 West, G.D., Perkins, J.M., Lewis, M.H.: Characterization of fine grained oxide ceramics, *J. Mat. Sci*., **39**, 6687-6704, (2004).

28 Krell, A., Strassburger, E.: Ballistic strength of opaque and transparent armor, *Am. Ceram. Soc. Bull.*, **86**(4), 9201-9207, (2007).

29 Hasselman, D.P.H.: Unified theory of thermal shock fracture initiation and crack propagation in brittle ceramics, *J. Am. Ceram. Soc.*, **52**(11), 600-604, (1969).

30 Gentilman, R.L.: Fusion casting of transparent spinel, *Am. Ceram. Soc. Bull.*, **60**(9), 906-909, (1981).

31 Lu, T.C., Chang, X.H., Qi, J.Q., Lou, X.J., Wei, Q.M., Sun, K., Wang, L.M.: Low temperature high pressure preparation of transparent nanocrystalline $MgAl_2O_4$ ceramics, *Appl. Phys. Lett.*, **88**, 213120-213123, (2006).

32 Morita, K., Kim, B-N., Hiraga, K., Yashida, H.: Fabrication of transparent $MgAl_2O_4$ spinel polycrystal by spark plasma sintering process, *Scripta Materialia*, **58**, 1114-1117, (2008).

33 Udalova, I.V., Maltzev, M.V., Petrik, V.I.: Transparent Spinel Ceramics. In: Proceeding of 3rd Euro Ceramics. Faenza Editrice Iberica, Madrid, (1993), **1**, 709-714.

34 Chang, X.H., Lu, T.C., Zhang, Y., Luo, X.J., Liu, Q., Huang, C.B., Qi, J.Q., Lei, M.Y., Huang, C.X., Lin, L.B.: $MgAl_2O_4$ transparent nano-ceramics prepared by sintering under ultra-high pressure, *Key Eng. Mat.,* **280-283**, 549-552, (2005).

35 Krell, A., Klimke, J., Hutzler, T.: Advanced spinel and sub-μm Al_2O_3 for transparent armor applications. *J. Eur. Ceram. Soc.*, **29**(2), 275-281, (2009).

36 Lange, F.F.: Sintering of agglomerated powders, *J. Am. Ceram. Soc.*, **67**(2), 83-89, (1984).

37 Rahaman, M.N.: Ceramic Processing and Sintering, 2nd edition. Marcel Dekker, New York, (2003).

38 Coble, R.L.: Sintering crystalline solids. I Intermediate and final state diffusion models, *J. App . Phys.*, **32**(5), 787-792, (1961).

39 Kang, S-J.L., Jung, Y-L.: Sintering kinetics at final stage sintering: model calculations and map construction, *Acta. Mat.*, **52**, 4573-4578, (2004).

40 Yan, M.F., Cannon, R.M., Bowen, H.K., Chowdhry, U.: Effect of grain size distribution on sintered density, *Mat. Sci. Eng.*, **60**, 275-281, (1983).

41 Helle, A.S., Easterling, K.E., Ashby, M.F.: Hot isostatic pressing diagrams: new developments, *Acta. Metall.*, **53**(12), 2163-2174, (1985).

42 Apetz, R., van Bruggen, M.P.B.: Transparent alumina: a light scattering model, *J. Am. Ceram. Soc.*, **86**(3), 480-486, (2003).

43 German, R.M.: Sintering Theory and Practice. J. Wiley & Sons, New York, (1996), p. 316.

44 Kwon, S.T., Kim, D.Y.: Effect of sintering temperature on the densification of Al_2O_3, *J. Am. Ceram. Soc.*, **70**(4), C69-C70, (1987).